Journal of Membrane Science 702 (2024) 122753



Contents lists available at ScienceDirect

Journal of Membrane Science

journal homepage: www.elsevier.com/locate/memsci





On the geometry and material stability of tubular PVDF-TiO_2 static mixer membrane contactors for photocatalytic ozonation of micropollutants

Stefan Herrmann [a], Franziska Ullrich [a], Maik Tepper [a,b], Matthias Wessling [a,b,*]

[a] RWTH Aachen University, AVT.CVT - Chair of Chemical Process Engineering, Forckenbeckstraße 51, 52074 Aachen, Germany
[b] DWI - Leibniz Institute for Interactive Materials, Forckenbeckstraße 50, 52074 Aachen, Germany

ARTICLE INFO

Keywords:
Helical static mixer membranes
Rotation-in-a-spinneret
Mixed matrix membranes
Photocatalytic ozonation
PVDF ozone stability

ABSTRACT

The prevention of ozone hotspots in ozonation reactors for wastewater treatment is essential for effective degradation of micropollutants without forming harmful by-products. Membrane contactors can provide a bubble-free ozonation process that is able to decrease by-product formation, e.g., bromate formation in bromide-charged wastewater. Furthermore, the geometry of the reactor influences the distribution of dissolved ozone in a membrane contactor. Turbulence promoters can significantly decrease ozone hotspots and increase ozone mass transfer into wastewater. This work presents a fabrication methodology to produce PVDF-TiO_2 helical static mixer membranes using the rotation-in-a-spinneret technology. Static mixer membranes combine the functionality of a membrane contactor and a static mixer in a single component. Furthermore, the PVDF matrix is doped with TiO_2 particles as photocatalyst. Thus, we present a membrane-based photocatalytic ozonation process to increase the concentration of hydroxyl radicals for degradation of micropollutants under UV radiation. Static mixer membranes increase the ozone mass transfer coefficient by 70% compared to conventional hollow fiber membranes. Furthermore, the specific photocatalytic degradation rate of methylene blue increases by 50% using static mixer membranes. However, this work also reveals a lack of long-term stability of PVDF-TiO_2 membranes in the corrosive environment of photocatalytic ozonation. The molecular weight of PVDF decreases by 11% after use in photocatalytic ozonation resulting in a loss of mechanical stability of the membranes. Similar material concepts are required based on ceramic materials which avoid wetting of the porosity.

1. Introduction

Clean water is fundamental for the existence of human life. With the emerging population, the demand for potable water is increasing, while the sources of clean water in nature are decreasing. To protect stable societies and human life, the supply of clean water is one of the Sustainable Development Goals of the United Nations [1]. However, aquatic environment pollution has increased in recent decades due to industrial and municipal wastewater [2,3].

Especially, the removal of micropollutants (MP) from wastewater is a challenge for conventional treatment processes. These MPs are persistent organic compounds, e.g., industrial chemicals such as per- and polyfluoroalkyl substances (PFAS) and pharmaceuticals [4–6]. Therefore, wastewater treatment plants (WWTP) are the main entrance point for MPs into surface waters [7,8]. Additional treatment stages in WWTPs are needed to prevent MPs from entering the environment. Advanced oxidation processes (AOP) are emerging for the removal of MPs in WWTPs and especially ozonation is intensively studied from lab-scale to full-scale application [7,9–11]. For ozone-based AOPs, ozone is dosed into the wastewater in bubble columns or Venturi injectors. These bubble-based processes have significant drawbacks, such as inhomogeneous ozone distribution, insufficient MP degradation, and formation of toxic or carcinogenic ozonation by-products, e.g., bromate in bromide-contaminated wastewater [12,13].

In contrast to bubble columns, membrane contactors are a viable reactor type for ozonation in a bubble-free process [14–20]. The bubble-free process allows precise dosing of ozone in wastewater and minimizes the amount of undissolved off-gas as it is produced in bubble columns. Undissolved ozone will remain in the reactor headspace and must be destroyed before it can be vented as oxygen off-gas [21,22]. Furthermore, membrane contactors show higher mass transfer coefficients than bubble columns and Venturi injectors [15]. Hydrophobic membrane materials show the highest mass transfer coefficient, fluorinated polymers, i.e., polytetrafluoroethylene (PTFE) and polyvinylidene fluoride (PVDF), the highest stability in corrosive media with gaseous and dissolved ozone, and hollow fiber membrane modules are

* Corresponding author at: RWTH Aachen University, AVT.CVT - Chair of Chemical Process Engineering, Forckenbeckstraße 51, 52074 Aachen, Germany.
E-mail address: Manuscripts.CVT@avt.rwth-aachen.de (M. Wessling).

https://doi.org/10.1016/j.memsci.2024.122753
Received 14 February 2024; Received in revised form 5 April 2024; Accepted 7 April 2024
Available online 10 April 2024
0376-7388/© 2024 The Author(s). Published by Elsevier B.V. This is an open access article under the CC BY license (http://creativecommons.org/licenses/by/4.0/).

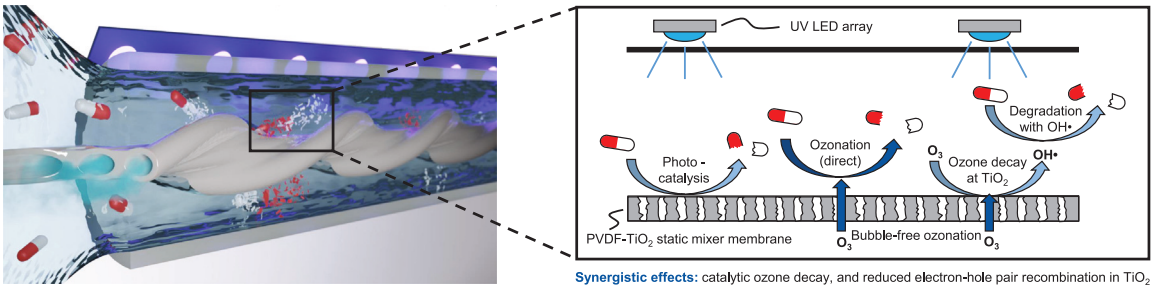


Fig. 1. Static mixer membranes with embedded photocatalyst for bubble-free photocatalytic ozonation of micropollutants. Gaseous ozone is applied to the lumen-side of the membrane, and micropollutant-contaminated water to the shell-side. LEDs provide UV light for photocatalysis through the glass housing. Micropollutants are degraded by three mechanisms: photocatalysis, reactions with ozone, and reactions with hydroxyl radicals and other oxidizing species, created either by reactions of water with electrons or electron holes of the photocatalyst, or by catalytic ozone decay at the photocatalyst.

advantageous over flat sheet membrane modules due to their higher specific surface area [15,23,24].

In literature, most membrane contactors for ozonation apply wastewater on the lumen-side of the membrane [17,19,20,25,26]. However, the water on the shell-side has advantages concerning the fouling behavior, as narrow lumen channels are prone to fouling in wastewater applications [16,27]. Furthermore, the importance of turbulence promotion in membrane modules for reduced fouling and enhanced mass transfer performance has been known for many years since Belfort et al. [28–30] and Fane et al. [31–33] studied the geometry influence of membranes and spacers on membrane performance. Additionally, the possible benefits of improved mixing for micropollutant degradation and mitigation of harmful by-products in ozonation are reported by Herrmann et al. in a previous publication [34]. However, this knowledge is barely used in the design of membranes and modules, which are still rather simple geometries today.

Instead of adding additional static mixers into a membrane contactor module, the membrane itself can be tailored in its geometry to promote mixing. Jani et al. [35] created mixing effects in hollow fibers with a curly geometry that induces Dean vortices in the lumen channel of the membrane [30,36]. The membrane modules were tested in a membrane contactor for oxygen absorption. An increase in oxygen flux into the water of 80% was measured, and enhanced mixing in the lumen channel was demonstrated with computational fluid dynamics (CFD) simulations. Sabelfeld et al. [25] used such curly PTFE membrane fibers for the ozonation of wastewater and showed up to 7 times increased ozone flux through the membrane due to enhanced mixing. Tepper et al. invented and patented [37] the rotation-in-a-spinneret technology to create hollow fiber membranes with helical ridges [38,39] on the lumen-side and to insert an additional static mixer into the lumen channel in-situ during the fabrication process of the membrane [40] for filtration and membrane contactor applications. Furthermore, Luelf et al. [41] developed a fabrication method for membranes in the shape of a twisted tape static mixer. Fig. 1 shows the geometry of such a static mixer membrane. This work uses the rotation-in-a-spinneret technology by Tepper et al. to fabricate static mixer membranes, similar to Luelf et al. for application in an ozonation process.

Besides the ozone mass transfer, the reaction mechanisms with MPs need to be optimized for an overall enhanced AOP. Ozone itself reacts selectively with some MPs while others are not degraded [42]. In contrast, hydroxyl radicals ($OH^{\cdot}$) react non-selectively with MPs with electron transfer, radical addition, and hydrogen abstraction mechanisms [42–44]. Thus, a high concentration of hydroxyl radicals and other unselective oxidizing species like $O2^{\cdot-}$ and $O3^{\cdot-}$ is favored for an efficient AOP. While ozone decay to hydroxyl radicals in water is comparably slow, particularly at acidic pH, other mechanisms can generate hydroxyl radicals more efficiently [45].

Photocatalytic ozonation combines ozonation and photocatalysis, showing synergistic effects in MP degradation [42]. Therefore, a photocatalyst, i.e., titanium dioxide, and a UV light source for its excitement are added to the ozonation process. In combination with a membrane contactor for ozonation, TiO_2 particles can be used as an immobilized catalyst in a mixed matrix membrane to create a photocatalytic ozonation process [46].

In photocatalytic ozonation, oxidizing species are created in many different parallel reactions, as shown in Fig. 2. Electrons (e^-) in the conduction band of the photocatalyst react with dissolved oxygen and ozone as well as in-situ produced hydrogen peroxide to $O2^{\cdot-}$, $O3^{\cdot-}$ and hydroxyl radicals, respectively. Electron holes (h^+) oxidize water to hydroxyl radicals at acidic conditions and OH^- ions to hydroxyl radicals at alkaline conditions. Furthermore, direct reactions of MPs with the photocatalyst and catalytic ozone decay, independent of UV radiation, occur. Additionally, photolysis creates $O^{\cdot}$ and hydroxyl radicals from dissolved ozone. The synergistic effects are based on reduced recombination of electron–hole pairs in the photocatalyst in the presence of ozone as an electron acceptor in the reaction to $O3^{\cdot-}$. [42,47,48]

Fernandes et al. use photocatalytic ozonation with optional H_2O_2 dosing for degradation of volatile organic compounds [50] and refinery effluents [51] in a pilot scale reactor with suspended catalyst. They can show synergistic effects and significantly enhanced degradation performance. Furthermore, Gomes et al. [52] use TiO_2 doped with noble metals for the degradation of parabens in water. They report enhanced degradation and reduced toxicity in the presence of a photocatalyst compared to ozonation with simultaneous UV radiation in the absence of a photocatalyst. He et al. [53] immobilized TiO_2 on a membrane and combined photocatalysis with ozonation through a membrane contactor on a microfluidic scale. Presumido et al. [54] used membrane-based photocatalytic ozonation on lab-scale. They created micro-sized ozone bubbles through their photocatalytic membrane for ozone input and studied the degradation of 19 micropollutants. However, in their system, photocatalytic ozonation did not increase the degradation of micropollutants due to short residence times.

This work presents a membrane-based, bubble-free photocatalytic ozonation process with increased mixing by the membrane's geometry, as shown in Fig. 1. We combine the technology of membrane contactors for bubble-free ozonation with photocatalytic membranes by fabricating tubular PVDF-TiO_2 mixed matrix membranes. Three hypotheses are to be proved in this work. First, dispersing additives are feasible to prevent the agglomeration of nanoparticles in the dope solution and to tune its viscosity. Second, the rotation-in-a-spinneret approach is suitable for the fabrication of mixed matrix membranes. Third, ozone mass transfer and specific photocatalytic degradation rate in photocatalytic ozonation are enhanced by using static mixer membranes.

2. Experimental

The fabrication method of PVDF-TiO_2 static mixer membranes using the rotation-in-a-spinneret technology is presented hereafter. Furthermore, the procedures for membrane characterization and membrane process experiments are shown.

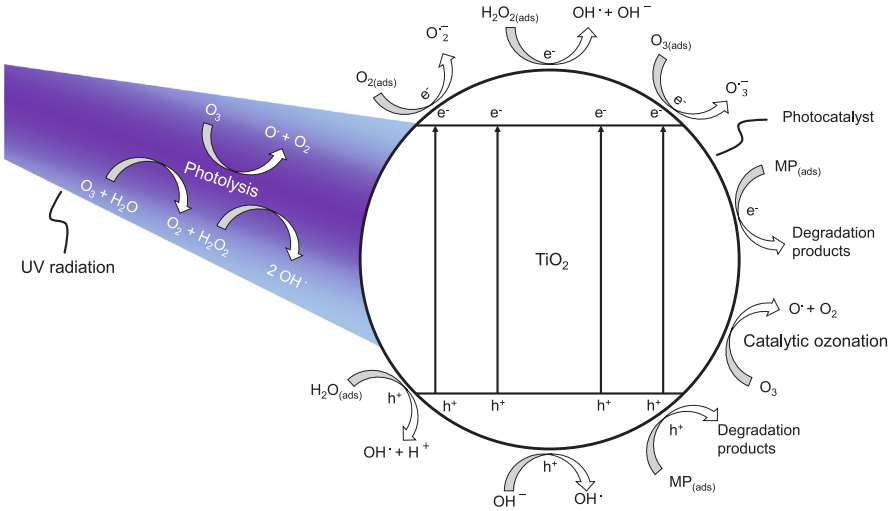


Fig. 2. Mechanisms of photocatalytic ozonation with TiO_2 as photocatalyst. The band gap of anatase TiO_2, is 3.2 eV; hence a wavelength of 387 nm or less is required to create electron–hole pairs in the material [49].

2.1. Membrane fabrication

Hollow fiber membranes are fabricated with a membrane-spinning device using a dry-wet spinning technique. Polyvinylidene fluoride (ABCR GmbH, Germany) is used as membrane material. N-methyl-2-pyrrolidon (NMP) (99%, Acros Organics, Belgium) is used as the solvent. Titanium dioxide powder (99.5%, Ionic Liquids Technologies GmbH, Germany) with anatase crystal configuration and a particle size of 20 nm, lithium chloride (LiCl) (≥99%, Sigma-Aldrich/Merck, Germany), and optional one of the dispersion additives Disperbyk-180, Disperbyk-111, or Disperplast-1142 (BYK-Chemie GmbH, Germany) is added to the dope solution. All chemicals are used without further purification. Table 1 lists the mass fractions of all dope solution ingredients. The use of 6.0 wt.-% TiO_2 nanoparicles in the dope solution results in approximately 36.0 wt.-% TiO_2 nanoparticles in dried membrane fibers. Dispersion additives are added at a ratio of 0.5 wt.-% to 3 wt.-% to the total mass of the dope solution.

Table 1
Basic dope solution for fabrication of single-bore and tri-bore hollow fiber membranes.

Component	Mass fraction wt.-%
PVDF	16.5
NMP	73.0
LiCl	3.5
TiO_2	6.0
DI water	1.0

The dope solution is prepared in two steps to avoid agglomeration of TiO_2 nanoparticles. First, dope solution part A is prepared with 75% of the NMP to dissolve LiCl and PVDF. LiCl is added to the solvent while stirring with a glass rod until dissolved. PVDF is poured in slowly under stirring to avoid the formation of PVDF powder agglomerates. To dissolve PVDF, the solution is mixed in a SpeedMixer (DAC600.2 CM153, Hauschild GmbH & Co. KG, Germany). The SpeedMixer runs for 30 s at 500 min^{-1}, then for 3.5 min at 1500 min^{-1}, and finally 1 min at 1000 min^{-1} in each run. The temperature of the solution increases up to 50 °C during this procedure. This program is repeated until PVDF has fully dissolved. Second, dope solution part B is prepared with the remaining 25% of NMP to form a suspension of TiO_2 particles. NMP, deionized (DI) water, and the dispersing additive are added into a beaker. The TiO_2 powder is ground with a coffee grinder to break larger agglomerates and then added into the beaker under stirring.

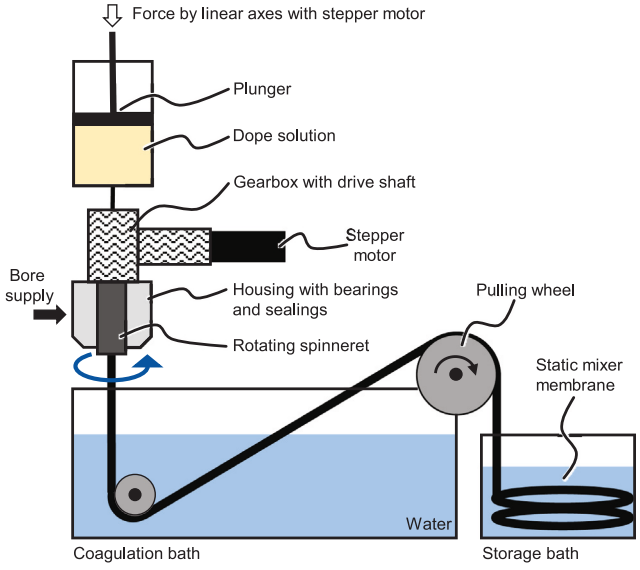


Fig. 3. Illustration of the membrane-spinning device for static mixer membranes, including the rotating spinneret, gearbox, and stepper motor. A plunger connected to a linear axes with a second stepper motor extrudes the dope solution from the dope vessel. A gear pump feeds the bore solution to the spinneret.

The solution is treated with a sonotrode (Ultrasonic Processor UP200S, Hielscher GmbH, Germany) at 65% amplitude and a cycle value of 0.8 for 2 h to form a suspension with non-agglomerated nanoparticles. Dope solutions A and B are then combined under slow stirring by hand and one SpeedMixer run with the above mentioned parameters is used to achieve a homogeneous dope solution. The dope solution is stored overnight for degassing and is used for spinning the next day.

Fig. 3 shows the membrane-spinning device with the dope vessel, the rotating spinning setup, the coagulation and storage baths, and the pulling wheel. A single-bore spinneret can replace the whole rotating spinning setup to produce standard single-bore membranes. Fig. 4 shows the two different spinnerets used to produce hollow fiber membranes in this work: a standard single-bore spinneret with one bore channel and a concentrically void for dope extrusion; and a tri-bore spinneret, adapted from Luelf et al. [41], for extrusion of tape-shaped hollow fiber membranes to produce static mixer membranes. Both spinnerets are 3D printed with a Form 3 (Formlabs, United States)

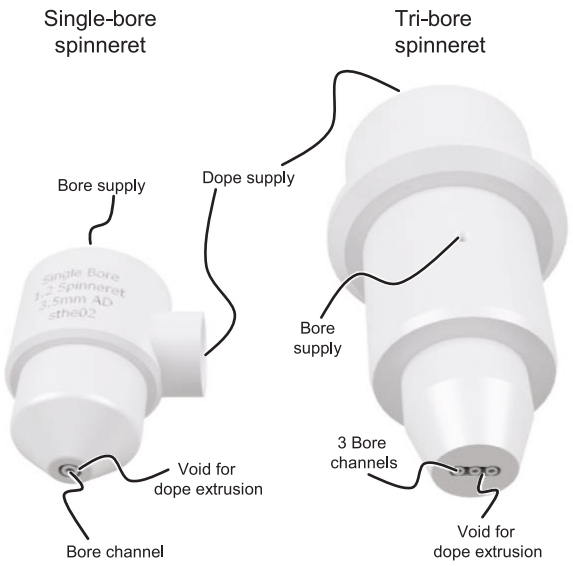


Fig. 4. Spinnerets used to produce single-bore hollow fibers (left) and static mixer membranes (right). The tri-bore spinneret is mounted into a housing during spinning, as shown in Fig. 5.

3D printer using Rigid resin (Formlabs, United States). The single-bore spinneret is directly placed into the spinning device, while the tri-bore spinneret needs to be mounted in a housing for the spinning process. The housing is connected to a gearbox, and a stepper motor, as shown in Fig. 5, to rotate the spinneret and create static mixer membranes.

The assembly of the static mixer membrane spinning setup, shown in Fig. 5 (a), contains an aluminum housing, two radial bearings (DIN 625) 16004 and 6007 (FAG, Schaeffler Technologies AG & Co. KG, Germany), two radial rotary shaft sealings (DIN 3760), separated by a distance ring, creating a rotational decoupling for supply of the bore solution to the spinneret, and circlips (DIN 472) to hold bearings and sealings in axial position. A hollow drive shaft is mounted to the spinneret with three M4 screws to connect it to the gearbox. The dope solution is supplied to the spinneret through the hollow drive shaft. After assembly of these parts, a gearbox connector plate is mounted onto the housing, and the housing is connected to the gearbox, as shown in Fig. 5 (b). The hollow drive shaft exits the gearbox at the top to connect the dope supply through a quick swivel joint GFS 18 (Landefeld GmbH, Germany). The gearbox DZA H, size 2 (Maedler GmbH, Germany), has a gear ratio of 1:1 and an angle of 90° between its axis. The input shaft of the gearbox is connected through a coupling MF-3648-NEMA23 (IGUS GmbH, Germany) to a stepper motor PD4-C5918L4204-E-01 (Nanotec Electronic GmbH & Co. KG, Germany). The setup, consisting of stepper motor, coupling, and gearbox, is adapted from Tepper et al. [38]. This setup allows to bring the rotational movement of the stepper motor to the spinneret inside its housing with rotational decoupling of dope and bore supply. The full bill of materials of the rotating spinning setup is presented in Table S1 in the supporting information. A 3D animation of the rotating spinning setup is presented in supplementary Video 1.

For spinning experiments with both spinnerets, a 1:1 mixture of DI water and NMP is used as bore solution to start the spinning process. When stable extrusion of a hollow fiber membrane is established, the bore fluid is changed to pure DI water. The air gap between the spinneret and precipitation bath is set to 50 mm. The precipitation bath is filled with DI water as non-solvent. The membranes are withdrawn from the precipitation bath with a pulling wheel. The fibers are stored in DI water for several days to allow full exchange of solvent and non-solvent before they are cut into pieces with a length of 0.6 m and dried at room temperature for several days.

2.2. Membrane characterization

Viscosity measurements of the dope solution are done with an MCR 302e (Anton Paar GmbH, Austria) rheometer. Dope solution samples are prepared as described above and measured without further preparation. All measurements are done by increasing the shear rate from $0.1\,s^{-1}$ to $1000\,s^{-1}$ and decreasing it back to $0.1\,s^{-1}$. All shown data is from the decreasing shear rate interval and averaged over three measurement repetitions.

Scanning electron microscopy (SEM) images are obtained with a SU 5000 FE-SEM (Hitachi Ltd., Japan). Membrane samples are dried for several days before SEM analysis. The fibers are submerged in isopropanol for 30 s and then placed in liquid nitrogen until adequately frozen. The frozen fibers are broken to obtain brittle fractures of the cross-section. SEM samples are sputtered with gold/palladium (ratio: 80/20) in a Q300TT (Quorum Technologies, United Kingdom) sputter coater prior to analysis. To visualize the TiO_2 distribution in the membrane matrix, energy dispersive X-ray spectroscopy (EDX) is used. Fiber samples are prepared similarly to SEM analysis without sputtering. A Quantax XFlash 6–60 (Bruker Corp., United States) is used for EDX analysis within the SEM.

Fourier-transform infrared spectroscopy (FTIR) is used to investigate the chemical structure of the membrane matrix. Dried membrane samples are placed on a GladiATR Diamond Frontier (Pike Technologies, United States) mounted to a Spectrum 3 (Perkin Elmer, United States) for analysis. All measurements are conducted in a wavenumber range from $400\,cm^{-1}$ to $4000\,cm^{-1}$.

Gel permeation chromatography (GPC) is used to measure the polymer's molecular weight distribution. Small samples of membrane fibers are dissolved in a $0.1\,mol\,L^{-1}$ LiCl in dimethylformamide (DMF) solution under stirring. The dissolved samples are filtered through a 200 nm syringe filter prior to analysis to prevent undissolved particles from entering the GPC columns. A pre-column and two GRAM columns with porosities of 30 Å and 1000 Å (PSS Polymer Standards Service GmbH, Germany) at a temperature of 45 °C with a $0.1\,mol\,L^{-1}$ LiCl in DMF solution as eluent are used for analysis. A refractive index detector Optilab Wrex-10 (Wyatt Technology Corp., United States) is used for data measurement.

For tensile strength measurements, membrane fibers are cut into pieces of 50 mm and glued into dedicated jigs on both ends with epoxy glue. The jigs are necessary to prevent deformation of the hollow fiber membrane ends by clamping into the measurement machine, as this would influence the elongation and fracture behavior of the membranes. The jigs are hooked into the Z005 (Zwick Roell GmbH & Co. KG, Germany) measurement machine. All tests are done with a preload of 0.08 N and a test speed of $5\,mm\,min^{-1}$.

2.3. Membrane process experiments

Membrane modules for mass transfer, photocatalytic, and advanced oxidation experiments are built with poly(methyl methacrylate) (PMMA) tubes (Röhm GmbH, Germany) with an inner diameter of 7 mm, an outer diameter of 10 mm, and a length of 250 mm. IQS tube fitting T-junctions (Sang-A Pneumatic Co. Ltd., Korea) connect the liquid inlet and outlet of the module. The membrane potting is done with hot glue and two-component epoxy glue 'UHU Plus Black' (UHU Holding GmbH, Germany). Modules with single-bore fibers are equipped with three fibers per module, while static mixer membrane modules are equipped with one fiber per module to ensure a comparable membrane surface within the modules.

The degradation of methylene blue is studied to characterize the photocatalytic activity of the membranes. A methylene blue (Carl Roth GmbH & Co. KG, Germany) solution with a concentration of $5\,mg\,L^{-1}$ is prepared with MilliQ water (Merck Millipore, United States) in a flask under stirring. The membrane module is used in a closed-loop configuration similar to Fig. 6 (a) but without connection to the ozone

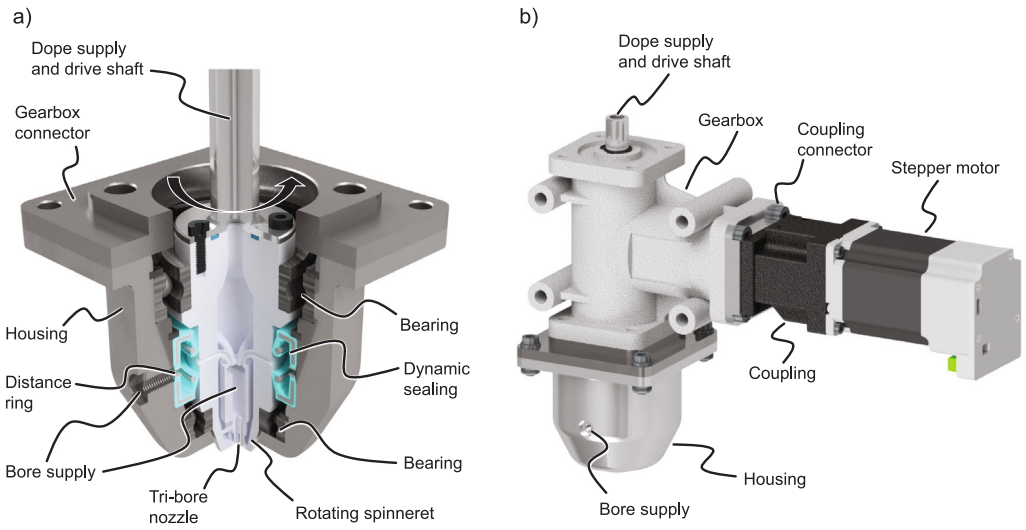


Fig. 5. Spinning setup for static mixer membranes. (a) 3D rendering of the tri-bore spinneret in its housing used to produce static mixer membranes. (b) 3D rendering of the rotating spinning setup, including spinneret, housing, drive shaft, gearbox, coupling, and stepper motor.

generator. All tubing in the experimental setup is made of PTFE. The reservoir is filled with 100 mL methylene blue solution, which is pumped through the shell-side of the membrane module at a flow rate of 150 mL min^{-1} by an MCP-Z process (Ismatec SA, Switzerland) gear pump with an MI0280 (Ismatec SA, Switzerland) pump head. The membrane module is placed in a self-made tubular UV reactor equipped with 30 UV-LEDs CUN6GF1 A (Seoul Viosys, Korea) with a total radiant flux of 42 W and a peak wavelength of 367 nm. The LEDs are arranged in three arrays with 10 LEDs each. The arrays are placed with an 120° offset around the membrane module for homogeneous irradiation of the membrane. Detailed information on the UV reactor can be found in a previous publication [55].

Nitrogen at a pressure of 50 mbar, adjusted with a back pressure regulator KBP1 (Swagelok, United Stated), is connected to the lumen-side of the membrane to ensure similar conditions at the phase boundary as in ozonation experiments. Photocatalytic experiments start with an adsorption phase of methylene blue onto the membrane fibers for 60 min. The UV reactor is switched off during this period. After the adsorption phase, the methylene blue solution is replaced with fresh stock solution, the UV reactor is switched on, and photocatalytic degradation starts. Samples are withdrawn from the stirred reservoir every 15 min for 2 h. The sample volume is approximately 1 mL. All samples are analyzed in a UV–VIS spectrometer U-5100 (Shimadzu Corp., Japan) at a wavelength of 664 nm. To consider differences in the surface area between single-bore and static mixer membrane modules, the specific MB degradation rate (SDR) is calculated with

$$\mathrm{SDR_{MB}} = \frac{\Delta c_{MB}}{\Delta t} \cdot \frac{1}{A_{mem}}$$

where $\frac{\Delta c}{\Delta t}$ is the change in MB concentration over time, and A_{mem} the surface area of the membranes per module.

An open-loop configuration, according to Fig. 6 (b), is used for ozone mass transfer experiments. An ozone generator BMT 802N (BMT Messtechnik GmbH, Germany) and an ozone analyzer BMT 964 (BMT Messtechnik GmbH, Germany) are used for ozone generation from pure oxygen (Westfalen AG, Germany) and measurement of the gaseous ozone concentration, respectively. All tubing in the experimental setup is made of ozone-stable PTFE. In all experiments, ozone is applied to the lumen-side of the membrane module at a concentration of 100 g N m^{-3} and a flow rate of approximately 14 L h^{-1}. Residual gaseous ozone is destructed by a manganese catalyst Carulite 200 (Lehmann & Voss & Co. KG, Germany). The dissolved ozone concentration in water is measured with cuvette tests LCK 310 (Hach Lange GmbH, Germany) and a DR 2800 photometer (Hach Lange GmbH, Germany). DI water is pumped through the membrane module with different flow rates between 100 mL min^{-1} and 200 mL min^{-1} at gaseous pressures between 0.1 bar and 0.2 bar. Gas and liquid side pressures can be adjusted with two back pressure regulators KBP1 (Swagelok, United States). The transmembrane pressure (TMP) is set to 0.1 bar for single-bore membrane fibers and 0.0 bar for static mixer membranes. The TMP is defined as

$$\mathrm{TMP} = p_L - p_g$$

where p_L is the liquid-side pressure and p_g is the gas-side pressure in the membrane module. Samples to measure the dissolved ozone concentration are withdrawn from a sample valve. The mass transfer coefficient K_L is calculated with

$$K_L = \frac{u}{a \cdot L} \cdot ln\left(\frac{c_g \cdot H_S^{cc}}{c_g \cdot H_S^{cc} - c_{l,out}}\right) = \frac{\dot{V}}{A_{mem}} \cdot ln\left(\frac{c_g \cdot H_S^{cc}}{c_g \cdot H_S^{cc} - c_{l,out}}\right)$$

where u is the liquid velocity, a the specific surface area of the membrane in the membrane module, L the effective length of the membrane module, c_g the gaseous ozone concentration, H_S^{cc} the Henry coefficient of ozone in water obtained from Sander [56], $c_{l,out}$ the dissolved ozone concentration at the outlet of the membrane module, $\dot{V}$ the volume flow rate of water, and A_{mem} the membrane surface area in the membrane module. The membrane surface area is calculated with the effective contact length in the membrane module and the circumference of the membrane fibers. The circumference is measured with a light microscope DMS 1000 (Leica Microsystems GmbH, Germany) and the related software LAS X.

Advanced oxidation experiments are conducted in closed-loop configuration according to Fig. 6 (a). Sulfamethoxazole (SMX) (analytical standard, Sigma-Aldrich/Merck, Germany) is used as a model micropollutant. A stock solution with a concentration of 0.08 mmol L^{-1} is prepared with MilliQ water in a beaker under stirring. 1 L of the stock solution is filled into the reservoir and used for a degradation experiment. The flow rate and concentration of ozone in the gas phase are similar to ozone mass transfer experiments. The liquid side flow rate is set to 150 mL min^{-1}. The UV reactor is turned off for sole ozonation experiments and switched on at a radiant power of 42 W for photocatalytic degradation and photocatalytic ozonation experiments. All experiments are run for 2 h, samples for high-performance liquid chromatography (HPLC) analysis with a volume of 1.5 mL are taken every 5 min, and total organic carbon (TOC) samples with a volume of 10 mL are taken every 30 min. The concentration of SMX in samples is measured with

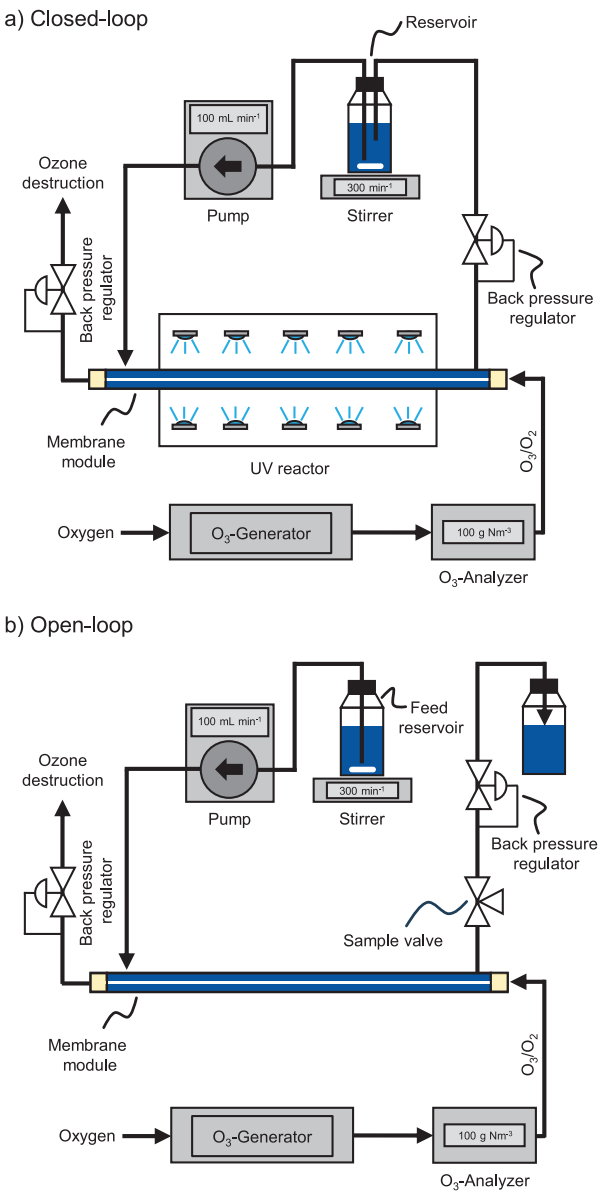


Fig. 6. Flow diagram of the experimental setup. (a) Closed-loop configuration used for methylene blue and micro-pollutant experiments. (b) Open-loop configuration used for ozone mass transfer measurements.

HPLC using a 1260 Infinity II with DAD MSD Quadrupole (Agilent Technologies Inc., United States). TOC samples are measured with a TOC-LCPH (Shimadzu Corp., Japan) using the difference method.

3. Results and discussion

First, the influence of dispersing additives on the dope solution properties for mixed matrix membrane fabrication is evaluated. Thereafter, the PVDF-TiO_2 static mixer membranes are studied in photocatalytic ozonation for MP degradation, and the material stability in a strongly oxidative environment is evaluated.

3.1. Dope solution formulation for mixed matrix membrane spinning

Producing mixed matrix membranes with nanoparticles arises challenges during the spinning process. The main challenges are the prevention of particle agglomerates and the viscosity of the dope solution. Here, TiO_2 nanoparticles are incorporated into the membrane matrix. The particles themselves have a diameter of around 20 nm; however, during transport and storage, they agglomerate to larger secondary particles in μm size. Particles this large block the spinneret during the spinning process and form large voids and defects in the membrane structure. Furthermore, they are inefficient for catalyst use, as most TiO_2 is encapsulated within an agglomerate without contact with UV light or micropollutants. Thus, agglomerated particles need to be separated and stabilized as single particles while preparing the dope solution. Separation can be successfully done by grinding and subsequent sonication, but a specific dispersing additive is needed to prevent forming of new agglomerates.

Three different dispersing additives optimized for use in NMP-based systems are tested, and their impact on membrane morphology is studied. 1.0 wt.-% of the dispersing additive Disperbyk 111, Disperbyk 180, or Disperplast 1142 is added to the dope solution during its preparation. It was possible to produce membrane fibers with all three additives, and no spinneret blocking occurred due to agglomerates. Fig. 7 shows FESEM pictures of single-bore hollow fiber membranes produced with the different dispersing additives. No TiO_2 agglomerates are visible, independent of the additive. Hence, the developed method of grinding and sonicating dope solution B can break up TiO_2 particle agglomerates, and dispersing additives can prevent the formation of new agglomerates within the dope solution. However, the membrane morphology varies with the dispersing additive used. Membranes produced with Disperbyk 180 and Disperplast 1142 form smooth surfaces on the lumen and shell-side. In contrast, the membrane produced with Disperbyk 111 has a deformed lumen-channel which is not favorable. The shell-side morphology is not significantly affected by the dispersing additive. All membranes show a thin nanoporous layer, with some larger pores, as can be seen for Disperbyk 111 and Disperplast 1142 in Fig. 7. Furthermore, membranes using Disperbyk 111 and Disperplast 1142 form a very dense structure in the center of the membrane matrix, increasing mass transfer resistance. The morphology of the membrane using Disperbyk 180 shows finger-like pores on the lumen and shell-side and a denser sponge-like structure in the center. Macrovoids towards the lumen-side further decrease the mass transfer resistance for gaseous ozone. The membrane requires no selectivity in a membrane contactor, so this morphology is favored. Subsequently, the distribution of TiO_2 particles within the membrane matrix is studied for hollow fibers with Disperbyk 180. Fig. 8 (b) shows the Ti-EDX-signal in a cross-section of the membrane with the related SEM picture in Fig. 8 (a). TiO_2 particles are evenly distributed through the membrane matrix and accessible on the shell-side of the membrane, as can be seen by the Ti-signal in the top right corner of the image, which shows the shell-side of the hollow fiber membrane. Thus, Disperbyk 180 is chosen as dispersing additive for all further experiments.

The viscosity of the dope solution is not only influenced by the particle load but also by the concentration of dispersing additive. Fig. 9 shows the viscosity of the dope solution at different concentrations of Disperbyk 180 between 0.0 wt.-% to 3.0 wt.-%. All tested dope solutions show shear thinning behavior, as the viscosity drops with increasing shear rates. The viscosity is lowered by 54% at low shear rates and 29% at high shear rates by using 0.5 wt.-% Disperbyk 180 compared to the dope solution without a dispersing additive. The change in viscosity by adding 1.0 wt.-% to 3.0 wt.-% is just 9% for low shear rates. The viscosity deviation increases for high shear rates. However, this might be an effect of the measurement method: the dope solution started to spill at shear rates exceeding 100 s^{-1}. Due to low expected shear rates in the spinneret, a concentration of 1.0 wt.-% is chosen, as a further increase of concentration does not significantly change the viscosity but increases the production cost of the membrane. In spinning experiments, dope solutions with 1.0 wt.-% Disperbyk 180 are successfully extruded without collapsing or bursting due to low viscosity. Furthermore, no dope flow rate limitations are discovered due to high viscosity and insufficient dope extrusion motor power.

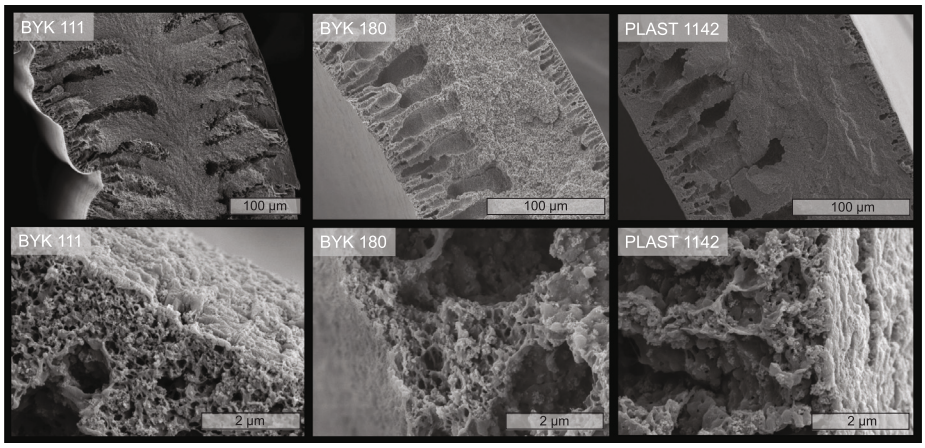


Fig. 7. FESEM pictures of single-bore membranes made with different dispersion additives: Disperbyk 111, Disperbyk 180, and Disperplast 1142.

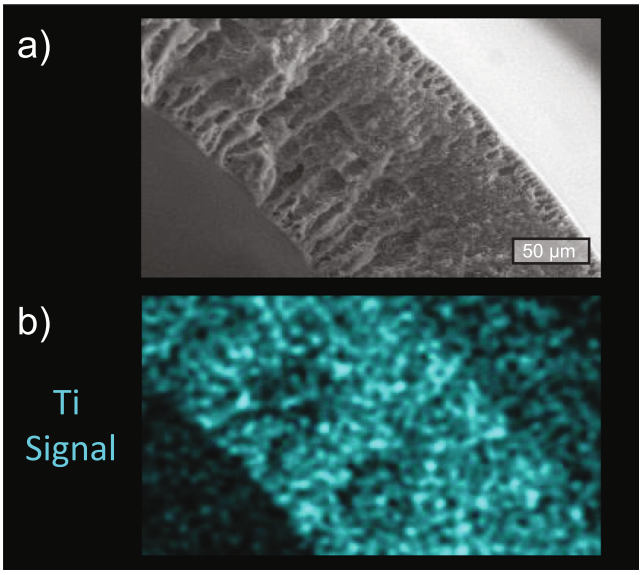


Fig. 8. EDX analysis of a PVDF-TiO_2 fiber with Disperbyk 180 as dispersing additive. (a) FESEM picture. (b) Corresponding EDX titanium signal.

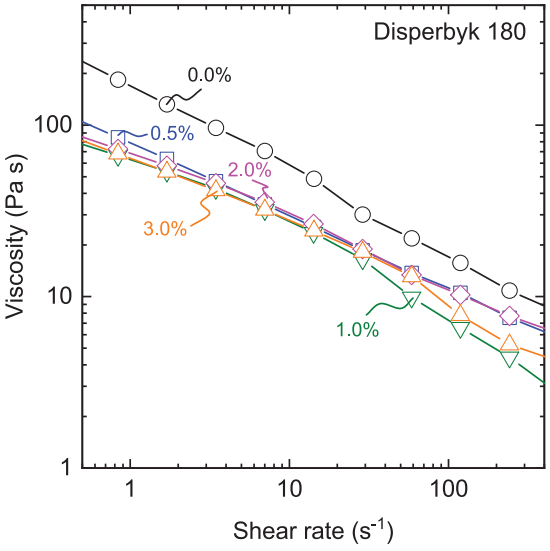


Fig. 9. Viscosity of the dope solution at room temperature over the shear rate for different Disperbyk 180 concentrations.

3.2. Fabrication of static mixer membranes

The viscosity-optimized dope solution makes it possible to produce static mixer membranes with a helical structure. The shear thinning behavior of the dope solution contributes to a stable fabrication process. The tape-like shape of the dope solution at the spinneret nozzle is fixed when the dope solution leaves the spinneret, as the shear rate suddenly drops after exiting the spinneret and the viscosity of the dope solution significantly increases. If the dope viscosity is too low and the shear thinning effect is insufficient, the geometry of the extruded fiber starts to change from a tape-like to a roundish shape, as the surface energy is minimized. In this case, a rotation of the spinneret does not lead to a helical shape on the shell-side of the fiber but to interwoven lumen channels on the inside of the hollow fiber.

Using a dope solution prepared according to Table 1 with 1.0 wt.-% Disperbyk 180 as dispersing additive enables the fabrication of helical-shaped static mixer membranes with TiO_2 particles as photocatalyst. The spinning process at different rotational speeds is shown in supplementary Video 2. The pitch length of the helix can be varied by changing the rotational speed of the spinneret. Fig. 10 (a) shows static mixer membranes extruded with rotational speeds from 0 min^{-1} to 40 min^{-1}. Without rotation of the spinneret, a simple tape is extruded from the spinneret. When rotation of the spinneret is started, a slight helical-shape is observed for a rotational speed of 10 min^{-1}. The helical structure becomes more explicit with increasing rotational speeds, and a visually appealing helix membrane is achieved at a rotational speed of 30 min^{-1}. Further increase of the rotational speed to 40 min^{-1} does not result in a helical-shaped membrane. The fiber has a roundish center with two small ridges that are wrapped around the center. Fig. 10 (b) shows the pitch length as a function of the rotational speed of the spinneret for membrane fibers before and after drying. The pitch length shows a linear relation to the rotational speed in a range between 20 min^{-1} and 40 min^{-1} for wet and dry fibers. The standard deviation of the pitch length decreases with higher rotational speeds, indicating a more stable spinning process. Furthermore, a shrinkage of the fibers can be observed during drying. Fibers tend to shrink more at lower rotational speeds during the spinning process with a shrinkage of 32% at 10 min^{-1} and just 22% at 40 min^{-1}.

Overall, using the spinning setup presented in Fig. 5 and dope solutions according to Table 1 with 1.0 wt.-% Disperbyk 180 enables the stable fabrication of helical-shaped static mixer membranes with a mixed matrix of PVDF and TiO_2. The influence of the pitch length on ozone mass transfer, photocatalytic behavior, and micropollutant degradation are studied subsequently.

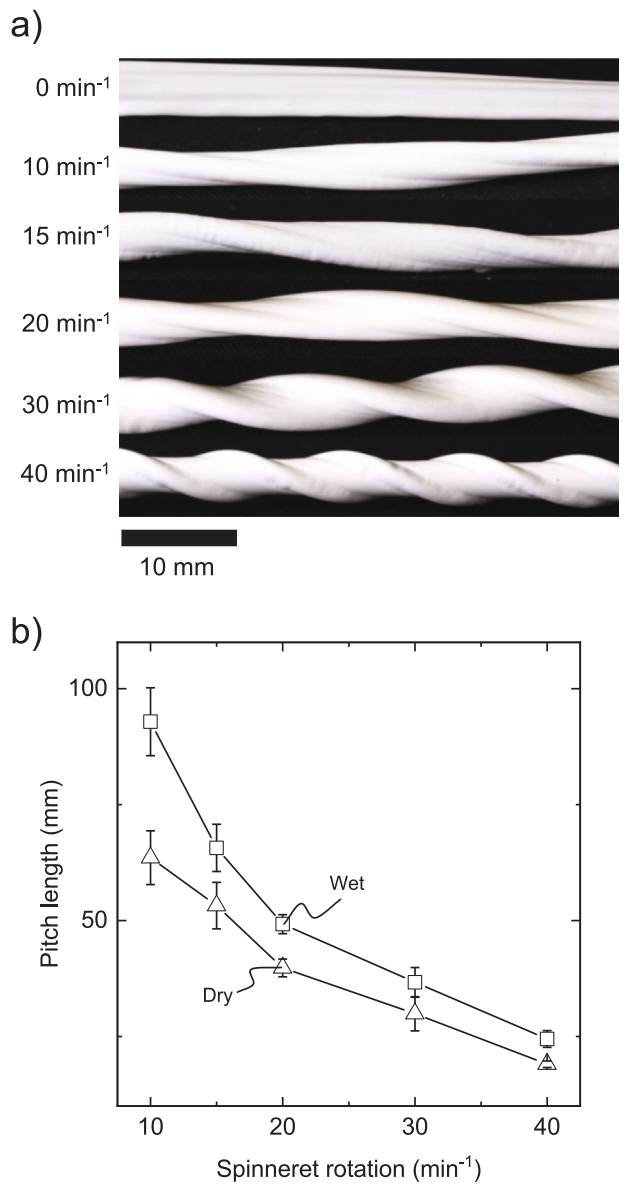


Fig. 10. Helical TiO_2-PVDF hollow fibers (static mixer membranes). (a) Pictures of the dried static mixer membranes fabricated at different rotational speeds of the spinneret. (b) Pitch length of wet and dry static mixer membranes over spinneret rotational speed. The error bars show the deviation of the pitch length within one fiber batch.

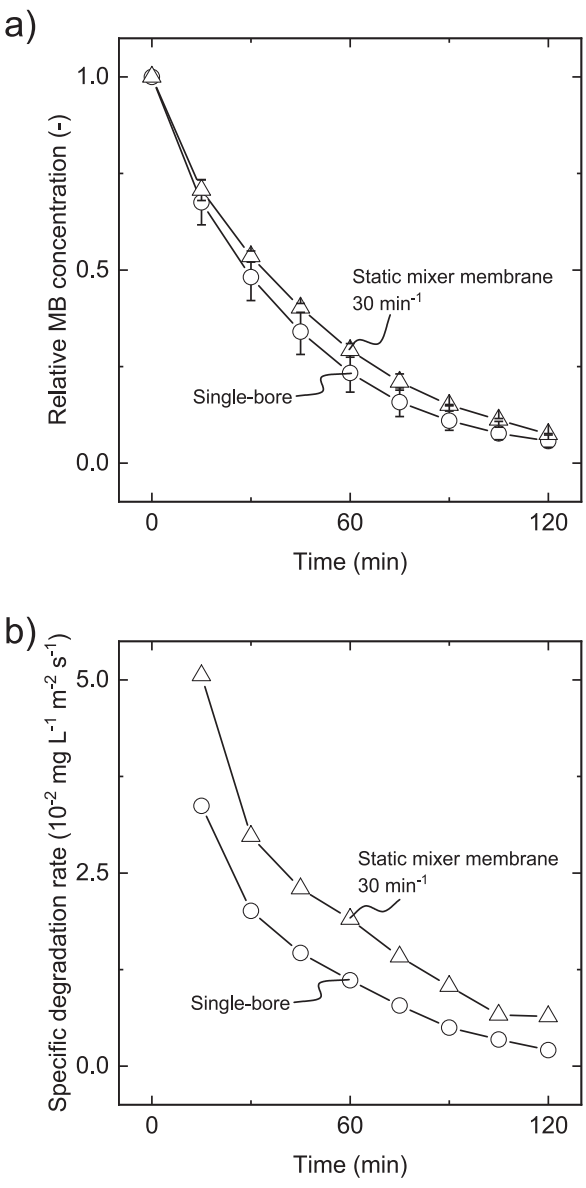


Fig. 11. Photocatalytic degradation of methylene blue (MB) with single-bore membranes and static mixer membranes. Experiments are conducted after an adsorption phase of 60 min. (a) Relative MB concentration over time. (b) Specific MB degradation rate related to the membrane surface area in the membrane module over time.

3.3. Characterization of static mixer membranes for photocatalysis and ozonation

The performance of static mixer membranes in photocatalytic methylene blue degradation is compared to single-bore membranes as a benchmark. Fig. 11 (a) shows the relative methylene blue concentration over time after the adsorption phase. The methylene blue degradation is 95% and 93% after 2 h for the single-bore membranes and static mixer membranes, respectively. Thus, the performance of the static mixer membrane is similar to the single-bore membrane taking the standard deviation into account. However, the surface area of the three membrane fibers in a single-bore module is estimated with $1.07 \times 10^{-2}\,m^2$ while the static mixer membrane module with a fiber spun at a rotational speed of $30\,min^{-1}$ has an estimated surface area of $6.4 \times 10^{-3}\,m^2$. Furthermore, no shadows, due to the fiber arrangement, which could decrease the effective surface area, were observed in the single-bore module. As the photocatalysis benefits from the 67% higher surface area of the single-bore fiber module, the direct comparison might not be ideal for performance evaluation. Thus, the specific MB degradation rate for both membrane modules is calculated to use the surface area of the modules for normalization. Fig. 11 (b) shows the specific degradation rate over time for single-bore and static mixer membrane modules. Taking the difference in surface area into account, the performance of static mixer membrane modules is advantageous compared to single-bore membrane modules. The specific degradation rate is significantly increased by 50% by static mixer membranes spun at $30\,min^{-1}$ at the beginning of a degradation experiment. The advantage of static mixer membranes further increases over the time of the experiment to over 200% after 120 min. This proves enhanced mixing in the membrane module due to the membrane acting as a static mixer. The contact probability of an MB molecule in the bulk phase with the photocatalytic surface is increased by the created radial flow components. Consequently, the degradation of MB increases.

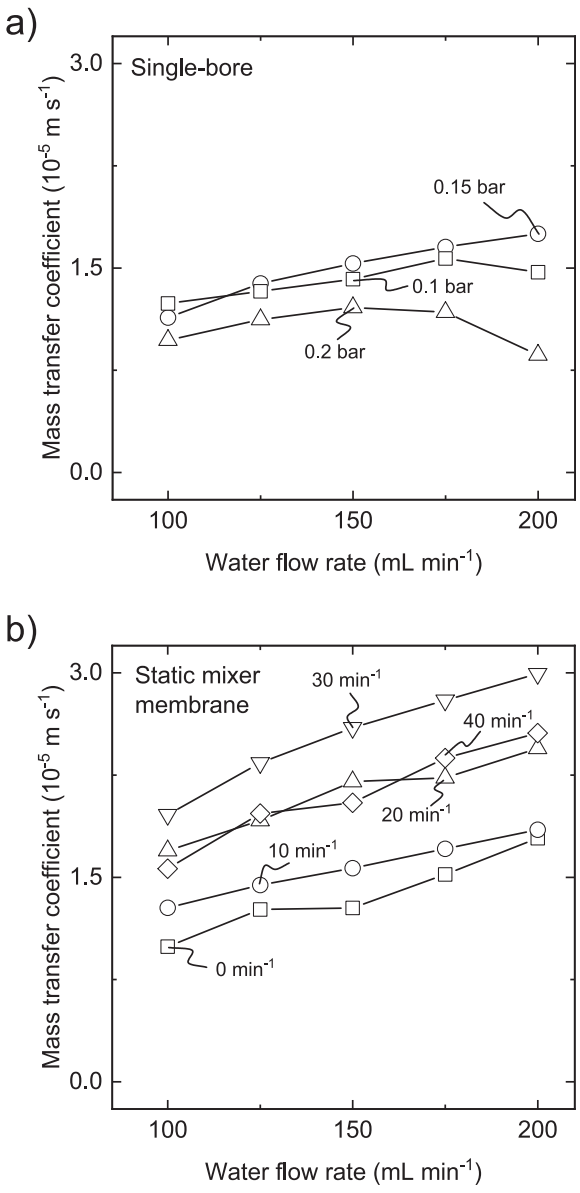


Fig. 12. Mass transfer coefficient for ozone in the membrane module. (a) Membrane module with three single-bore fibers at a constant TMP of 0.1 bar and varying gas-side pressure. (b) Membrane modules with one static mixer membrane fabricated at different rotational speeds at a constant TMP of 0.0 bar and a gas-side pressure of 0.1 bar.

Open-loop ozonation experiments are conducted to assess the mass transfer performance of static mixer membranes. The ozone concentration at the membrane contactor outlet is measured, and the mass transfer coefficient is calculated. Fig. 12 shows the mass transfer coefficient for (a) single-bore modules for different water flow rates and gas-side pressures and (b) static mixer membrane modules for different water flow rates and helix pitch lengths. Experiments with single-bore modules are done with varying gas-side pressures between 0.1 bar and 0.2 bar at constant TMP. By increasing the pressure from 0.1 bar to 0.15 bar, the mass transfer coefficient is slightly increased at high flow rates. However, further pressure increase to 0.2 bar significantly decreases the mass transfer coefficient. The liquid-side pressure is set to 0.3 bar in this experiment. Hence, a shift of the phase boundary is assumed and first wetting of the membrane pores occurs, hindering the mass transfer. Overall, the mass transfer coefficient for single-bore modules is in the order of 1.5×10^{-5} m s^{-1}. For static mixer membrane modules, the first bubble point and liquid entry pressure change, most likely due to changes in pore size or pore shape by the fabrication method with the rotational spinneret. A stable phase boundary is observed at a TMP of 0.0 bar and a gas-side pressure of 0.1 bar. The mass transfer coefficient for static mixer membrane modules increases with increasing rotational speed during membrane spinning. Static mixer membranes fabricated at 0 min^{-1} and 10 min^{-1} show similar mass transfer coefficients as single-bore modules. An improvement of mass transfer is obtained for fibers fabricated at 20 min^{-1}, 30 min^{-1}, and 40 min^{-1} over the whole range of water flow rates. A maximum of mass transfer is obtained with modules built with 30 min^{-1} static mixer membranes. Here, the mass transfer coefficient is increased by up to 98% compared to static mixer membranes fabricated with 0 min^{-1} and by 70% compared to single-bore fibers at 0.15 bar. The increase in the mass transfer coefficient is explained by the induced radial flow components on the liquid-side, creating convective ozone transport from the membrane's surface into the bulk phase. This lowers the liquid-side ozone concentration at the membrane and increases the driving force of mass transfer, the concentration gradient between the gas-side and liquid-side. Further increased rotational speed during membrane fabrication does not result in improved mass transfer. Static mixer membranes fabricated with 40 min^{-1} changed the shape from a helix shape to a roundish shape, as discussed before. The change in shape decreases the mixing performance and the mass transfer of the membrane.

In conclusion, a significant advantage in ozone mass transfer and photocatalytic degradation is obtained by the static mixer membranes fabricated at a rotational speed of 30 min^{-1} due to improved radial mixing within the membrane module.

3.4. Micropollutant degradation with static mixer membranes

The overall aim of the membrane development in this work is to use the membranes in an advanced oxidation process, combining ozonation with photocatalysis to increase the amount of hydroxyl radicals in the membrane contactor for enhanced micropollutant degradation. Therefore, static mixer membranes spun at 30 min^{-1} are used for SMX degradation experiments. SMX is a micropollutant that can directly react with ozone and hydroxyl radicals for degradation and is classified as highly oxidizable in literature [57,58]. Fig. 13 (a) shows the relative SMX concentration over time for photocatalytic degradation, sole ozonation and photocatalytic ozonation. As TiO_2 is also present in the static mixer membrane in ozonation experiments, this is already a catalyzed ozonation process.

The photocatalytic ozonation process is expected to increase the concentration of hydroxyl radicals. Thus, the degradation of SMX within the reactor should be accelerated. However, the experimental results show the opposite behavior. The degradation of SMX using photocatalytic ozonation is slower compared to sole ozonation. While complete degradation of SMX is achieved after 90 min with sole ozonation, after 120 min with photocatalytic ozonation still 11% of the total SMX is present. The sole photocatalytic degradation is significantly slower and results in a degradation of just 12% after 120 min.

Fig. 13 (b) shows the corresponding relative TOC concentration in water during the experiments. For photocatalytic degradation, the TOC is relatively constant over time. This is expected due to the low SMX degradation shown in Fig. 13 (a). A significant decrease in TOC is expected for the other two processes, as SMX is mostly or completely degraded. However, ozonation experiments reveal a slight increase in TOC to 150% of its initial value after 120 min. The increase in TOC can only be explained by the degradation of PVDF in the membrane matrix and the leaching of organic components into water. The PVDF degradation effect by ozonation may be more significant than expected from the TOC increase shown in Fig. 13 (a), compared to photocatalytic degradation. Here, the PVDF degradation by ozonation is overlaid by complete SMX degradation and a resulting decrease in TOC. For photocatalytic ozonation, the TOC increase is even worse as it increases to

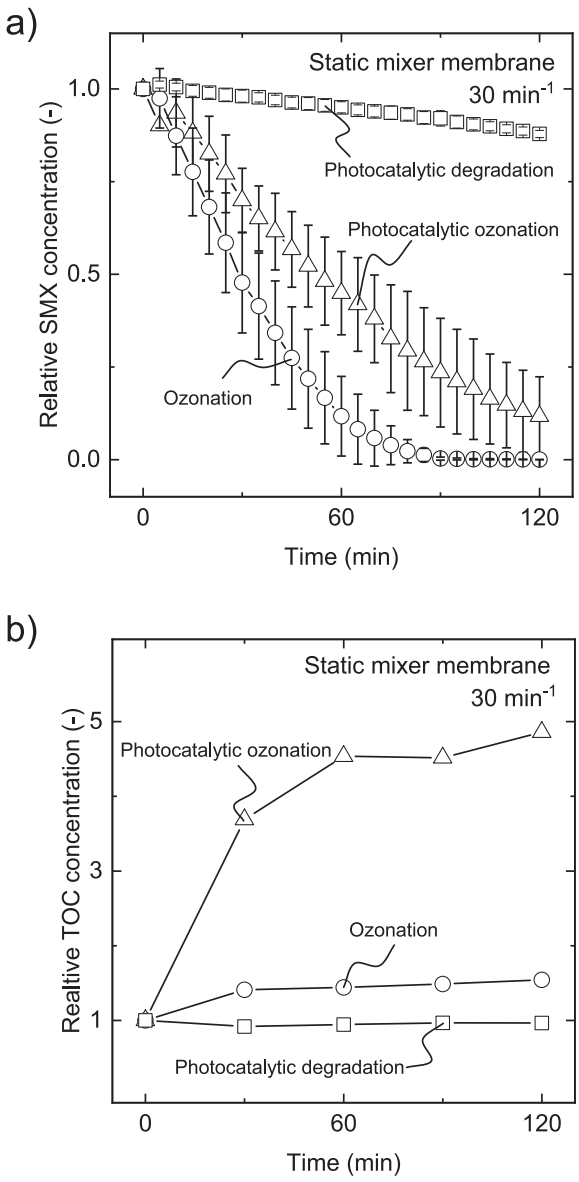


Fig. 13. Degradation of sulfamethoxazole (SMX) with static mixer membrane modules with sole ozonation and photocatalytic ozonation. (a) Relative concentration of SMX over time. (b) Relative total organic carbon (TOC) concentration over time.

nearly 500% of its initial value. This indicates a significant degradation of the PVDF-TiO_2 membrane. The degradation of PVDF could also explain the large error bars in SMX degradation, as the degradation reaction seems to differ slightly for each membrane module used in the experiments.

Hence, it is assumed that ozone and hydroxyl radicals are degrading parts of the membrane contactor, resulting in organic carbon leaching into the water. As the leaching behavior is increased by photocatalytic ozonation, it is assumed that the concentration of highly reactive hydroxyl radicals increases with this process. Competition between multiple parallel reactions can also explain the slower SMX degradation using photocatalytic ozonation, as the amount of hydroxyl radicals and ozone molecules reacting with SMX decreases when they react with other materials in the membrane contactor. Furthermore, the lifetime of hydroxyl radicals is limited in the range of μs. The concentration decreases from the location of their generation significantly towards the bulk phase within nm to μm. Thus it is likely that materials are attacked by oxidizing species in the direct surrounding where they are formed [59,60]. On the one hand, ozone decay generates hydroxyl radicals in the bulk phase. However, in MilliQ water with a low SMX concentration, the rate of ozone decay to hydroxyl radicals is expected to be low at neutral pH [45]. On the other hand, hydroxyl radicals are formed at the photocatalyst on the membrane's surface. As the TOC increase is significant for photocatalytic ozonation, hydroxyl radicals most likely degrade the membrane. Furthermore, the membrane becomes brittle after use in photocatalytic ozonation.

Altogether, even though the performance of the static mixer membrane regarding ozone mass transfer and photocatalytic degradation was superior to single-bore membranes, the overall membrane matrix containing PVDF as polymer seems not suitable for a process in harsh conditions with high concentrations of hydroxyl radicals around the membrane.

3.5. Ozone stability of PVDF-tio$_2$ membranes

PVDF is reported in the literature as an ozone-stable material. However, changes in material properties like tensile strength and performance loss of PVDF membranes are reported for long-term use under ozone exposure [15,23,61]. The membrane modules in this work are used for several experiments over 2 h to 3 h each. They are investigated for changes in chemical and mechanical properties after use in photocatalytic ozonation experiments to evaluate the stability of the membranes in a corrosive environment, including gaseous ozone, dissolved ozone, and hydroxyl radicals. Therefore, membrane fibers of the same fabrication batch are compared before and after the use in photocatalytic ozonation experiments.

Fig. 14 (a) compares FTIR spectra of pristine fibers and fibers used in photocatalytic ozonation. The spectra are normalized to the characteristic PVDF peak at 1176 cm^{-1}. All characteristic peaks of PVDF and the β-PVDF crystal structure remain unchanged at 1403 cm^{-1}, 1176 cm^{-1}, 1074 cm^{-1}, 880 cm^{-1}, and 1431 cm^{-1} 1277 cm^{-1} 840 cm^{-1}, respectively. The stability of these peaks to ozonation is also reported in literature [62–64]. However, for both fiber geometries the broad peak at 650 cm^{-1} shifts to higher waver numbers with a maximum at 720 cm^{-1}, indicating degradation within the membrane matrix. Furthermore, the strong peak between 450 cm^{-1} and 400 cm^{-1} increases its intensity proportional to the PVDF peak at 1176 cm^{-1} after use of fibers in photocatalytic ozonation. The peak corresponds to TiO_2 nanoparticles in the membrane matrix. The intensity increase indicates a higher amount of TiO_2 at the membrane surface, visible for FTIR, that might result from a decreasing amount of PVDF at the membrane surface due to PVDF degradation by hydroxyl radicals formed at the incorporated photocatalyst. Furthermore, there are indications that PVDF degradation also appears in sole photocatalytic experiments. FTIR spectra of fibers used in photocatalytic experiments are presented in Figure S1 in the supplementary information. Changes in the FTIR spectrum are observed for wavenumbers of 650 cm^{-1} and below on the shell-side surface, while the lumen-side surface remains unchanged. However, the changes are less pronounced compared to photocatalytic ozonation.

Fig. 14 (b) shows the molecular weight distribution of PVDF before and after use in photocatalytic ozonation. The peak shift to lower molecular weights is observed during exposure to ozone and hydroxyl radicals. The mass averaged molecular weight M_w decreases by 11% from 3.435×10^5 g mol^{-1} for the pristine material to 3.063×10^5 g mol^{-1} after photocatalytic ozonation. Thus, polymer chains in the membrane matrix are degraded by the corrosive conditions in the membrane contactor. This supports the FTIR analysis that indicated degradation within the polymer matrix. The degradation of PVDF itself can also explain the rising TOC in SMX degradation experiments with photocatalytic ozonation. Furthermore, the membrane degradation creates a competition between polymer matrix and micropollutant degradation for hydroxyl radicals that reduces the micropollutant degradation in photocatalytic ozonation experiments.

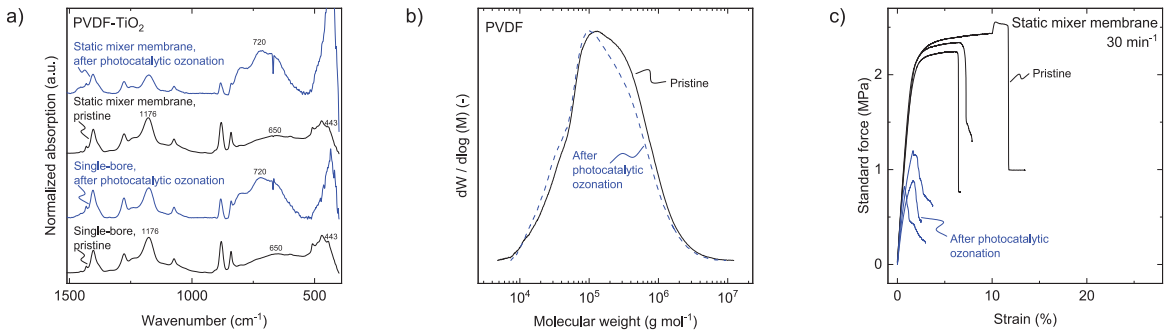


Fig. 14. Changes in membrane fibers after photocatalytic ozonation experiments. (a) FTIR spectra before and after photocatalytic ozonation experiments. Spectra are normalized to the characteristic PVDF peak at 1176 cm^{-1}. (b) Molecular weight distribution of PVDF before and after photocatalytic ozonation experiments. (c) Tensile tests of pristine static mixer membranes and static mixer membranes used in photocatalytic ozonation experiments.

Fig. 14 (c) presents tensile tests conducted with static mixer membranes before and after use in photocatalytic ozonation. A significant decrease in elongation at break and maximum force is obtained after the fibers are exposed to ozone and hydroxyl radicals. Single-bore fibers show similar behavior with a significant decrease in elongation at break. Li et al. [63] reported similar results of decreasing mechanical stability of PVDF membranes during ozonation. However, it remains unclear if the drop in mechanical strength in their material results from PVDF degradation or degradation of the used, non-fluorinated support. Here, the membrane matrix consists only of PVDF, TiO_2, and a small amount of the dispersing additive Disperbyk 180. Thus, the reduction in tensile strength is explained by the degradation of PVDF, as indicated by the decreasing molecular weight and change in FTIR spectra.

Overall, it is shown that the PVDF-TiO_2 membrane is not long-term stable in photocatalytic ozonation, which results in a high hydroxyl radical concentration directly at the membrane's surface. The lack of long-term stability is not only affecting the mechanical strength of the membrane but also the degradation of micropollutants in the membrane contactor as a competition for hydroxyl radicals is created between micropollutant degradation and membrane degradation.

4. Conclusions

This work presents a spinning setup to produce helical-shaped PVDF-TiO_2 membranes that combine the functions of a membrane contactor and a static mixer. Furthermore, a method to prevent agglomeration of nanoparticles in dope solutions for membrane fabrication is developed. Disperbyk 180 is used as a dispersing additive that enables the fabrication of photocatalytic static mixer membranes with a homogeneous distribution of TiO_2 nanoparticles in the polymer matrix.

It is shown that static mixer membranes can increase the initial specific degradation rate of methylene blue by 50% compared to single-bore hollow fiber membranes. Furthermore, ozonation using static mixer membranes increases the mass transfer coefficient of 70%. These results prove the importance of radial mixing in a membrane contactor.

In addition, static mixer membranes are studied in photocatalytic ozonation regarding their MP degradation behavior. It is shown that SMX can be degraded with sole ozonation and photocatalytic ozonation. However, the degradation of SMX is slower using photocatalytic ozonation. It is shown that the increased amount of hydroxyl radicals, generated with photocatalytic ozonation, degrades the membrane itself and slows down the micropollutant degradation. A 11% decrease in molecular weight of PVDF, a significant decrease in tensile strength, and changes in the FTIR spectrum after exposure to photocatalytic ozonation are shown. Thus, it is concluded that PVDF-TiO_2 membranes are not long-term stable in a corrosive environment with a high hydroxyl radical concentration created at the PVDF surface.

Despite the insufficient material stability for photocatalytic ozonation, the static mixer membranes can be used in other applications to utilize the benefits of an increased mass transfer coefficient. Possible applications are membrane contactors for oxygenation or carbon dioxide capture, and catalytic reaction systems consisting of an aqueous and gaseous phase in a less oxidative environment.

CRediT authorship contribution statement

Stefan Herrmann: Conceptualization, Methodology, Investigation, Visualization, Writing – original draft, Writing – review & editing. **Franziska Ullrich:** Investigation, Validation, Writing – original draft. **Maik Tepper:** Methodology, Supervision, Writing – review & editing. **Matthias Wessling:** Conceptualization, Project administration, Funding acquisition, Writing – review & editing.

Declaration of competing interest

The authors declare that they have no known competing financial interests or personal relationships that could have appeared to influence the work reported in this paper.

Data availability

Data will be made available on request.

Acknowledgments

M.W. acknowledges DFG funding through the Gottfried Wilhelm Leibniz Award 2019 (WE 4678/12-1). The authors thank Timo Linzenmeier, Justin Gottfried, and Frederike Schiszler for the analysis of a large amount of HPLC samples, Karin Faensen for FESEM pictures and viscosity measurements, Lennart Wilms and Konstantin Dietz for supporting experiments and TOC analysis, Nick Semrau for supporting GPC measurements, Karl Heidmann for supporting 3D renderings, Laura Schlieger, Tim Gebhardt and Tamara Tschepe for preliminary experiments. Dispersing additives were kindly provided by BYK-Chemie GmbH.

Appendix A. Supporting information

Supplementary material related to this article can be found online at https://doi.org/10.1016/j.memsci.2024.122753.

References

[1] UN General-Assembly, Transforming our world: the 2030 agenda for sustainable development, 70/1, 2015, United Nations URL https://sdgs.un.org/2030agenda.

[2] N.M. Kumar, M.C. Sudha, T. Damodharam, S. Varjani, Micro-pollutants in surface water: Impacts on the aquatic environment and treatment technologies, in: Current Developments in Biotechnology and Bioengineering, Elsevier, 2020, pp. 41–62, http://dx.doi.org/10.1016/B978-0-12-819594-9.00003-6.

[3] A. Pal, Y. He, M. Jekel, M. Reinhard, K.Y.-H. Gin, Emerging contaminants of public health significance as water quality indicator compounds in the urban water cycle, Environ. Int. 71 (2014) 46–62, http://dx.doi.org/10.1016/j.envint.2014.05.025.

[4] Forever Pollution Project, Journalists tracking PFAS across Europe, 2023, URL https://foreverpollution.eu/.

[5] H.A. Kaboré, S. Vo Duy, G. Munoz, L. Méité, M. Desrosiers, J. Liu, T.K. Sory, S. Sauvé, Worldwide drinking water occurrence and levels of newly-identified perfluoroalkyl and polyfluoroalkyl substances, Sci. Total Environ. 616–617 (2018) 1089–1100, http://dx.doi.org/10.1016/j.scitotenv.2017.10.210.

[6] World Health Organization, Pharmaceuticals in drinking-water, 2012.

[7] D. Kanakaraju, B.D. Glass, M. Oelgemöller, Advanced oxidation process-mediated removal of pharmaceuticals from water: A review, J. Environ. Manage. 219 (2018) 189–207, http://dx.doi.org/10.1016/j.jenvman.2018.04.103.

[8] J.-Q. Jiang, Z. Zhou, V.K. Sharma, Occurrence, transportation, monitoring and treatment of emerging micro-pollutants in waste water — A review from global views, Microchem. J. 110 (2013) 292–300, http://dx.doi.org/10.1016/j.microc.2013.04.014.

[9] R. Dewil, D. Mantzavinos, I. Poulios, M.A. Rodrigo, New perspectives for advanced oxidation processes, J. Environ. Manage. 195 (Pt 2) (2017) 93–99, http://dx.doi.org/10.1016/j.jenvman.2017.04.010.

[10] K. Ikehata, Y. Li, Ozone-based processes, in: Advanced Oxidation Processes for Waste Water Treatment, Elsevier, 2018, pp. 115–134, http://dx.doi.org/10.1016/B978-0-12-810499-6.00005-X.

[11] M. Bourgin, B. Beck, M. Boehler, E. Borowska, J. Fleiner, E. Salhi, R. Teichler, U. von Gunten, H. Siegrist, C.S. McArdell, Evaluation of a full-scale wastewater treatment plant upgraded with ozonation and biological post-treatments: Abatement of micropollutants, formation of transformation products and oxidation by-products, Water Res. 129 (2018) 486–498, http://dx.doi.org/10.1016/j.watres.2017.10.036.

[12] R. Wünsch, T. Hettich, M. Prahtel, M. Thomann, T. Wintgens, U. von Gunten, Tradeoff between micropollutant abatement and bromate formation during ozonation of concentrates from nanofiltration and reverse osmosis processes, Water Res. 221 (2022) 118785, http://dx.doi.org/10.1016/j.watres.2022.118785.

[13] E.C. Wert, F.L. Rosario-Ortiz, D.D. Drury, S.A. Snyder, Formation of oxidation byproducts from ozonation of wastewater, Water Res. 41 (7) (2007) 1481–1490, http://dx.doi.org/10.1016/j.watres.2007.01.020.

[14] A. Mansourizadeh, I. Rezaei, W.J. Lau, M.Q. Seah, A.F. Ismail, A review on recent progress in environmental applications of membrane contactor technology, J. Environ. Chem. Eng. 10 (3) (2022) 107631, http://dx.doi.org/10.1016/j.jece.2022.107631.

[15] E. Bein, I. Zucker, J.E. Drewes, U. Hübner, Ozone membrane contactors for water and wastewater treatment: A critical review on materials selection, mass transfer and process design, Chem. Eng. J. 413 (2021) 127393, http://dx.doi.org/10.1016/j.cej.2020.127393.

[16] A. Schmitt, J. Mendret, S. Brosillon, Evaluation of an ozone diffusion process using a hollow fiber membrane contactor, Chem. Eng. Res. Des. 177 (2022) 291–303, http://dx.doi.org/10.1016/j.cherd.2021.11.002.

[17] T. Merle, W. Pronk, U. von Gunten, MEMBRO 3 X, a novel combination of a membrane contactor with advanced oxidation (O 3 /H 2 O 2) for simultaneous micropollutant abatement and bromate minimization, Environ. Sci. Technol. Lett. 4 (5) (2017) 180–185, http://dx.doi.org/10.1021/acs.estlett.7b00061.

[18] D.S. Pines, K.-N. Min, S.J. Ergas, D.A. Reckhow, Investigation of an ozone membrane contactor system, Ozone Sci. Eng. 27 (3) (2005) 209–217, http://dx.doi.org/10.1080/01919510590945750.

[19] T. Leiknes, J. Phattaranawik, M. Boller, U. von Gunten, W. Pronk, Ozone transfer and design concepts for NOM decolourization in tubular membrane contactor, Chem. Eng. J. 111 (1) (2005) 53–61, http://dx.doi.org/10.1016/j.cej.2005.05.007.

[20] R. Jansen, J.W. de Rijk, A. Zwijnenburg, M. Mulder, M. Wessling, Hollow fiber membrane contactors—A means to study the reaction kinetics of humic substance ozonation, J. Membr. Sci. 257 (1–2) (2005) 48–59, http://dx.doi.org/10.1016/j.memsci.2004.07.038.

[21] H. Schaar, M. Clara, O. Gans, N. Kreuzinger, Micropollutant removal during biological wastewater treatment and a subsequent ozonation step, Environ. Pollut. (Barking, Essex : 1987) 158 (5) (2010) 1399–1404, http://dx.doi.org/10.1016/j.envpol.2009.12.038.

[22] L. Debevec, A review of ozone generating facilities in some U.S. water and wastewater treatment plants, Ozone Sci. Eng. 12 (2) (1990) 95–105, http://dx.doi.org/10.1080/01919519008552212.

[23] F.R.A.d. Santos, C.P. Borges, F.V. Da Fonseca, Polymeric materials for membrane contactor devices applied to water treatment by ozonation, Mater. Res. 18 (5) (2015) 1015–1022, http://dx.doi.org/10.1590/1516-1439.016715.

[24] E. Chabanon, E. Favre, 3.9 Membranes contactors for intensified gas–liquid absorption processes, in: Comprehensive Membrane Science and Engineering, Elsevier, 2017, pp. 249–281, http://dx.doi.org/10.1016/B978-0-12-409547-2.12250-4.

[25] M. Sabelfeld, S.-U. Geißen, Effect of helical structure on ozone mass transfer in a hollow fiber membrane contactor, J. Membr. Sci. 574 (2019) 222–234, http://dx.doi.org/10.1016/j.memsci.2018.10.056.

[26] G. Zoumpouli, R. Baker, C. Taylor, M. Chippendale, C. Smithers, S. Xian, D. Mattia, Y. Chew, J. Wenk, A single tube contactor for testing membrane ozonation, Water 10 (10) (2018) 1416, http://dx.doi.org/10.3390/w10101416.

[27] I.G. Wenten, H. Julian, N.T. Panjaitan, Ozonation through ceramic membrane contactor for iodide oxidation during iodine recovery from brine water, Desalination 306 (2012) 29–34, http://dx.doi.org/10.1016/j.desal.2012.08.032.

[28] G. Belfort, Fluid mechanics in membrane filtration: Recent developments, J. Membr. Sci. 40 (2) (1989) 123–147, http://dx.doi.org/10.1016/0376-7388(89)89001-5.

[29] H.B. Winzeler, G. Belfort, Enhanced performance for pressure-driven membrane processes: the argument for fluid instabilities, J. Membr. Sci. 80 (1) (1993) 35–47, http://dx.doi.org/10.1016/0376-7388(93)85130-O.

[30] M.E. Brewster, K.-Y. Chung, G. Belfort, Dean vortices with wall flux in a curved channel membrane system, J. Membr. Sci. 81 (1–2) (1993) 127–137, http://dx.doi.org/10.1016/0376-7388(93)85037-W.

[31] A.R. Da Costa, A.G. Fane, Net-type spacers: Effect of configuration on fluid flow path and ultrafiltration flux, Ind. Eng. Chem. Res. 33 (7) (1994) 1845–1851, http://dx.doi.org/10.1021/ie00031a026.

[32] J. Schwinge, D.E. Wiley, A.G. Fane, R. Guenther, Characterization of a zigzag spacer for ultrafiltration, J. Membr. Sci. 172 (1–2) (2000) 19–31, http://dx.doi.org/10.1016/S0376-7388(00)00312-4.

[33] Z. Cao, D.E. Wiley, A.G. Fane, CFD simulations of net-type turbulence promoters in a narrow channel, J. Membr. Sci. 185 (2) (2001) 157–176, http://dx.doi.org/10.1016/S0376-7388(00)00643-8.

[34] S. Herrmann, M.C. Padligur, C.J. Bieneck, M. Wessling, Modeling of tubular membrane contactors for ozonation of water reveals reduced bromate formation with static mixers, Chem. Eng. Sci. 291 (2024) 119924, http://dx.doi.org/10.1016/j.ces.2024.119924.

[35] J.M. Jani, M. Wessling, R.G. Lammertink, Geometrical influence on mixing in helical porous membrane microcontactors, J. Membr. Sci. 378 (1–2) (2011) 351–358, http://dx.doi.org/10.1016/j.memsci.2011.05.021.

[36] P. Moulin, J.C. Rouch, C. Serra, M.J. Clifton, P. Aptel, Mass transfer improvement by secondary flows: Dean vortices in coiled tubular membranes, J. Membr. Sci. 114 (2) (1996) 235–244, http://dx.doi.org/10.1016/0376-7388(95)00323-1.

[37] M.W. Maik Tepper, Membrane system, spinneret for manufacturing the membrane system, device including the spinneret and method for forming the membrane system: EP 3808435, 2021, URL https://patents.google.com/patent/EP3808435A1/de?oq=EP3808435A1.

[38] M. Tepper, L. Fehlemann, J. Rubner, T. Luelf, H. Roth, M. Wessling, Rotating microstructured spinnerets produce helical ridge membranes to overcome mass transfer limitations, J. Membr. Sci. 643 (2022) 119988, http://dx.doi.org/10.1016/j.memsci.2021.119988.

[39] M. Tepper, M. Padligur, D. Wypysek, L. Budeus, J. Mueller-Dott, H. Roth, M. Wessling, Helical-ridge-membranes from PVDF for enhanced gas–liquid mass transfer, J. Membr. Sci. 673 (2023) 121471, http://dx.doi.org/10.1016/j.memsci.2023.121471.

[40] M. Tepper, Y. Eminoglu, N. Mehling, J. Walorski, H. Roth, M. Wessling, Rotation-in-a-Spinneret integrates static mixers inside hollow fiber membranes, J. Membr. Sci. 656 (2022) 120599, http://dx.doi.org/10.1016/j.memsci.2022.120599.

[41] T. Luelf, D. Rall, D. Wypysek, M. Wiese, T. Femmer, C. Bremer, J.U. Michaelis, M. Wessling, 3D-printed rotating spinnerets create membranes with a twist, J. Membr. Sci. 555 (2018) 7–19, http://dx.doi.org/10.1016/j.memsci.2018.03.026.

[42] M. Mehrjouei, S. Müller, D. Möller, A review on photocatalytic ozonation used for the treatment of water and wastewater, Chem. Eng. J. 263 (2015) 209–219, http://dx.doi.org/10.1016/j.cej.2014.10.112.

[43] C. von Sonntag, The basics of oxidants in water treatment. Part A: OH radical reactions, Water Sci. Technol. 55 (12) (2007) 19–23, http://dx.doi.org/10.2166/wst.2007.383.

[44] C. von Sonntag, U. von Gunten, Chemistry of Ozone in Water and Wastewater Treatment: From Basic Principles to Applications, IWA Publishing, 2012, http://dx.doi.org/10.2166/9781780400839.

[45] D. Gardoni, A. Vailati, R. Canziani, Decay of ozone in water: A review, Ozone Sci. Eng. 34 (4) (2012) 233–242, http://dx.doi.org/10.1080/01919512.2012.686354.

[46] S. Liu, E. Véron, S. Lotfi, K. Fischer, A. Schulze, A.I. Schäfer, Poly(vinylidene fluoride) membrane with immobilized TiO2 for degradation of steroid hormone micropollutants in a photocatalytic membrane reactor, J. Hazard. Mater. 447 (2023) 130832, http://dx.doi.org/10.1016/j.jhazmat.2023.130832.

[47] M.N. Chong, B. Jin, C.W.K. Chow, C. Saint, Recent developments in photocatalytic water treatment technology: a review, Water Res. 44 (10) (2010) 2997–3027, http://dx.doi.org/10.1016/j.watres.2010.02.039.

[48] J. Nawrocki, B. Kasprzyk-Hordern, The efficiency and mechanisms of catalytic ozonation, Appl. Catal. B 99 (1–2) (2010) 27–42, http://dx.doi.org/10.1016/j.apcatb.2010.06.033.

[49] C. Dette, M.A. Pérez-Osorio, C.S. Kley, P. Punke, C.E. Patrick, P. Jacobson, F. Giustino, S.J. Jung, K. Kern, TiO2 anatase with a bandgap in the visible region, Nano Lett. 14 (11) (2014) 6533–6538, http://dx.doi.org/10.1021/nl503131s.

[50] A. Fernandes, M. Gagol, P. Makoś, J.A. Khan, G. Boczkaj, Integrated photocatalytic advanced oxidation system (TiO2/UV/O3/H2O2) for degradation of volatile organic compounds, Sep. Purif. Technol. 224 (2019) 1–14, http://dx.doi.org/10.1016/j.seppur.2019.05.012.

[51] A. Fernandes, P. Makoś, Z. Wang, G. Boczkaj, Synergistic effect of TiO2 photocatalytic advanced oxidation processes in the treatment of refinery effluents, Chem. Eng. J. 391 (2020) 123488, http://dx.doi.org/10.1016/j.cej.2019.123488.

[52] J.F. Gomes, I. Leal, K. Bednarczyk, M. Gmurek, M. Stelmachowski, M. Diak, M. Emília Quinta-Ferreira, R. Costa, R.M. Quinta-Ferreira, R.C. Martins, Photocatalytic ozonation using doped TiO2 catalysts for the removal of parabens in water, Sci. Total Environ. 609 (2017) 329–340, http://dx.doi.org/10.1016/j.scitotenv.2017.07.180.

[53] X. He, R. Chen, X. Zhu, Q. Liao, L. An, X. Cheng, L. Li, Optofluidics-based membrane microreactor for wastewater treatment by photocatalytic ozonation, Ind. Eng. Chem. Resear. 55 (31) (2016) 8627–8635, http://dx.doi.org/10.1021/acs.iecr.6b00562.

[54] P.H. Presumido, R. Montes, J.B. Quintana, R. Rodil, M. Feliciano, G.L. Puma, A.I. Gomes, V.J. Vilar, Ozone membrane contactor to intensify gas/liquid mass transfer and contaminants of emerging concern oxidation, J. Environ. Chem. Eng. 10 (6) (2022) 108671, http://dx.doi.org/10.1016/j.jece.2022.108671.

[55] S. Herrmann, L.T. Hirschwald, K.H. Heidmann, J. Linkhorst, M. Wessling, Lab-scale tubular LED UV reactor for continuous photocatalysis, HardwareX 17 (2024) e00506, http://dx.doi.org/10.1016/j.ohx.2023.e00506.

[56] R. Sander, Compilation of Henry's law constants (version 5.0.0) for water as solvent, Atmos. Chem. Phys. 23 (19) (2023) 10901–12440, http://dx.doi.org/10.5194/acp-23-10901-2023.

[57] B. Mathon, M. Coquery, Z. Liu, Y. Penru, A. Guillon, M. Esperanza, C. Miège, J.-M. Choubert, Ozonation of 47 organic micropollutants in secondary treated municipal effluents: Direct and indirect kinetic reaction rates and modelling, Chemosphere 262 (2021) 127969, http://dx.doi.org/10.1016/j.chemosphere.2020.127969.

[58] S. Willach, H.V. Lutze, K. Eckey, K. Löppenberg, M. Lüling, J. Terhalle, J.-B. Wolbert, M.A. Jochmann, U. Karst, T.C. Schmidt, Degradation of sulfamethoxazole using ozone and chlorine dioxide - compound-specific stable isotope analysis, transformation product analysis and mechanistic aspects, Water Res. 122 (2017) 280–289, http://dx.doi.org/10.1016/j.watres.2017.06.001.

[59] J.A. LaVerne, The production of OH radicals in the radiolysis of water with 4 He ions, Radiat. Res. 118 (2) (1989) 201, http://dx.doi.org/10.2307/3577437.

[60] S. Zhang, M. Sun, T. Hedtke, A. Deshmukh, X. Zhou, S. Weon, M. Elimelech, J.-H. Kim, Mechanism of heterogeneous fenton reaction kinetics enhancement under nanoscale spatial confinement, Environ. Sci. Technol. 54 (17) (2020) 10868–10875, http://dx.doi.org/10.1021/acs.est.0c02192.

[61] S. Bamperng, T. Suwannachart, S. Atchariyawut, R. Jiraratananon, Ozonation of dye wastewater by membrane contactor using PVDF and PTFE membranes, Sep. Purif. Technol. 72 (2) (2010) 186–193, http://dx.doi.org/10.1016/j.seppur.2010.02.006.

[62] C.S. Raota, S. Lotfi, R. Lyubimenko, B.S. Richards, A.I. Schäfer, Accelerated ageing method for the determination of photostability of polymer-based photocatalytic membranes, J. Membr. Sci. (2023) 121944, http://dx.doi.org/10.1016/j.memsci.2023.121944.

[63] K. Li, W. Xu, G. Wen, Z. Zhou, M. Han, S. Zhang, T. Huang, Aging of polyvinylidene fluoride (PVDF) ultrafiltration membrane due to ozone exposure in water treatment: Evolution of membrane properties and performance, Chemosphere 308 (Pt 3) (2022) 136520, http://dx.doi.org/10.1016/j.chemosphere.2022.136520.

[64] S. Uličná, M. Owen-Bellini, S.L. Moffitt, A. Sinha, J. Tracy, K. Roy-Choudhury, D.C. Miller, P. Hacke, L.T. Schelhas, A study of degradation mechanisms in PVDF-based photovoltaic backsheets, Sci. Rep. 12 (1) (2022) 14399, http://dx.doi.org/10.1038/s41598-022-18477-1.